





# Electrical conductivity of QGP with quasiparticle quarks and Gribov gluon

Sadaf Madni<sup>1</sup> , Sumit<sup>2</sup> , Lata Thakur<sup>3,4</sup> , Najmul Haque<sup>1</sup> 

<sup>1</sup> School of Physical Sciences, National Institute of Science Education and Research, An OCC of Homi Bhabha National Institute, Jatni-752050, India

<sup>2</sup> School of Physics, Beijing Institute of Technology, 102488 Beijing, China

<sup>3</sup> Department of Physics and Institute of Physics and Applied Physics, Yonsei University, Seoul 03722, Korea

<sup>4</sup> Asia Pacific Center for Theoretical Physics, Pohang, Gyeongbuk 37673, Republic of Korea

Received: date / Accepted: date

**Abstract** We investigate the electrical conductivity of the quark–gluon plasma (QGP) using a non-perturbative resummation scheme incorporating the Gribov-modified gluon propagator. The electrical conductivity is evaluated by solving the relativistic Boltzmann transport equation within the relaxation-time approximation, where the relaxation times are obtained from microscopic two-body scattering amplitudes. A quasiparticle description is employed for quarks, providing a unified framework for studying transport properties across both weakly and strongly coupled regimes. Above the deconfinement transition temperature, we estimate the electrical conductivity of the QGP and compare our results with available lattice QCD data and various phenomenological models, finding good agreement with the lattice results.

## 1 Introduction

The discovery of the quark–gluon plasma (QGP) at the beginning of this century has opened new directions in the study of strongly interacting matter through relativistic heavy-ion collision (HIC) experiments at RHIC and the LHC [1–3]. One of the principal objectives of these experimental programs is to obtain precise estimates of the transport properties of the QGP. Over the past two decades, extensive theoretical and phenomenological studies employing ideal [4–8], viscous hydrodynamics [9–15] have revealed that the QGP is a strongly coupled system behaving as an almost perfect fluid in HICs. The hydrodynamic description of QGP provides

valuable insights into its evolution and transport characteristics [16–18].

Transport properties, characterized by the corresponding transport coefficients, encode essential information about microscopic interactions within the medium and serve as crucial theoretical inputs for the hydrodynamic modeling of QGP. These coefficients are indispensable for analyzing HIC data and understanding the dynamical properties of QGP [17, 19, 20].

In relativistic HIC, extremely strong electromagnetic fields are also generated [21]. The influence of these fields on QGP dynamics, however, remains a topic of active debate. Some studies suggest that the fields decay rapidly with time and thus have limited impact on the medium’s evolution, while others argue that a finite electrical conductivity can significantly prolong their lifetime, potentially leading to observable effects. Once local equilibrium is established, the electrical conductivity ( $\sigma_{el}$ ) of the medium becomes a key parameter governing how electromagnetic fields evolve and interact with the plasma. The electrical conductivity of QGP has been extensively studied within various theoretical frameworks [22–51]. During the early stage of the collision, electric currents are generated by the quarks, with  $\sigma_{el}$  governing this production process. The value of  $\sigma_{el}$  plays a fundamental role in determining the strength of the chiral magnetic effect [52], which is a signature of CP violation in strong interactions [53]. In mass asymmetric collisions (such as Cu–Au collisions), the electrical field has a preferred direction, which generates a charge asymmetric flow [34]. The strength of this flow is directly related to  $\sigma_{el}$ , which is associated with the emission rate of soft photons [54, 55].

In this work, we compute the electrical conductivity of the QGP medium using the Gribov-Zwanziger (GZ) approach [56, 57]. This approach has gained sig-

<sup>1</sup>E-mail: sadaf.madni@niser.ac.in

<sup>2</sup>E-mail: sumit@ph.iitr.ac.in

<sup>3</sup>E-mail: thakurphyom@gmail.com

<sup>4</sup>E-mail: nhaque@niser.ac.in

nificant attention, particularly after its generalization to finite temperature QCD medium [58, 59]. Studies have shown that the infrared mass scale parameter,  $\gamma_G$  which is an intrinsic Yang-Mills scale, originally introduced by Gribov to explain the non-perturbative confinement region, significantly improves the infrared behavior of QCD and leads to a good agreement with lattice results for thermodynamic quantities [60] along with the novel massless excitations ascribable to the magnetic scale [61]. The Gribov dispersion relation provides a simple way to account for the effects of residual confinement on the transport properties of the QGP. It was first used in Refs. [62–64] in the context of kinetic theory and hydrodynamics, where it was applied to a boost-invariant setup. Also, its impact on observables, such as the dilepton rate and quark number susceptibility, has been examined [65]. Additionally, the shear and bulk viscosity of the QGP medium have been explored using Gribov gluons and quasiparticle quarks [66] along with mesonic screening masses [67], spectral sum rules for quarks [68], and the different properties of heavy quark sector [69–73], have also been investigated using the GZ scheme. Recently, a covariant kinetic theory has been developed to study the transport coefficients for Gribov plasma [74]. The study utilized a quasiparticle-like framework with bag correction for pressure and energy density. The temperature dependence of the Gribov parameter was obtained from pure gauge lattice thermodynamics [74], whereas the running coupling was fixed using the (2 + 1)-flavor lattice QCD equation of state. We have utilized these parameters in this work to calculate the electrical conductivity of the QGP medium.

This article is divided into six sections. Section 2 discusses the formalism of the current work in detail, where the Gribov parameter and running coupling,  $g$ , are defined. Section 3 focuses on the scattering cross-section of the constituent particles and computes the scattering amplitude of quark-quark and quark-antiquark interaction. In Section 4, the relaxation time is revisited, which is based on the weighted thermally averaged quark-quark and quark-antiquark cross-section. Section 5 investigates the electrical conductivity of the medium by utilizing the quasiparticle model. Finally, Section 6 provides an overview and outlook of the work.

## 2 Formalism

### 2.1 Gribov parameter and running coupling

The Gribov-modified gluon propagator, in the Landau gauge, reads [61]

$$\mathcal{D}_{ab}^{\mu\nu}(k) = \delta_{ab} \frac{k^2}{k^4 + \gamma_G^4} \left( \delta^{\mu\nu} - \frac{k^\mu k^\nu}{k^2} \right), \quad (1)$$

where  $k^\mu$  is the Euclidean gluon four momentum, and the temperature dependence of the Gribov parameter is determined from pure gauge lattice thermodynamics [74]. Note that the Gribov parametrization has been extensively studied in the literature to explain deconfined nuclear matter [58–65].

It is important to realize that in this work, we have employed the general form of the Gribov-modified gluon propagator (Eq. (1)) to evaluate the electrical conductivity of the QGP medium. For simplicity and to focus on the primary effects of the Gribov modification, we have neglected any contributions from gluon condensate terms in the propagator, which would lead to the emergence of a dynamical mass term (see Ref. [76]). It is important to note that recent lattice studies indicate a preference for the so-called decoupling solution, where the gluon propagator remains finite in the limit  $k \rightarrow 0$ . This behavior can be incorporated into a more refined version of the GZ framework that includes such condensate effects, leading to a modified propagator with a dynamical mass term. However, incorporating these refinements introduces additional complexities and model dependencies that are beyond the scope of the present work. Here, we opt to use the original Gribov form of the gluon propagator without these condensate-induced modifications. This choice allows us to isolate the impact of the Gribov parameter on the electrical conductivity. It provides a clear and straightforward framework for understanding its effects on the QGP's transport properties. While this approach represents a simplified treatment, it serves as a baseline study to elucidate the key features of Gribov-modified gluons in QGP without the additional complications arising from dynamical mass terms.

To characterize the system's dynamics, the energy-momentum tensor takes on the following form [74, 75]

$$T_{(0)}^{\mu\nu} = \int dk \cdot k^\mu k^\nu g^0 + B_0(T) g^{\mu\nu}, \quad (2)$$

where  $B_0(T)$  is bag pressure, which is added to take care of thermodynamic consistency in equilibrium,  $g^{\mu\nu}$  is the metric tensor where  $g^{\mu\nu} = \text{diag}(+1, -1, -1, -1)$  and  $g^0$  is the equilibrium distribution function for Gribov plasma, with  $g_\pm^0$  corresponding to the two dispersion branches, defined as,

$$g_\pm^0 = \frac{1}{e^{\epsilon_\pm/T} - 1}, \quad (3)$$

where  $\epsilon_\pm = \sqrt{|\mathbf{k}|^2 \pm i\gamma_G^2}$  with  $|\mathbf{k}|$  as the three-momentum of the gluons. The Lorentz invariant momentum integral is given by

$$\int dk = \frac{d_g}{(2\pi)^3} \int d^3\mathbf{k} \int dk_0 \, 2 \times \Theta(k_0) \delta\left(k^2 + \frac{\gamma_G^4}{k^2}\right). \quad (4)$$

In the above equation, the degeneracy factor,  $d_g = 2 \times (N_c^2 - 1) = 16$ . Note that in the Landau gauge, the Gribov framework also comes with ghost degrees of freedom. At very large temperatures, these ghost degrees of freedom cancel a longitudinal gluon mode that contributes to the expression of the free-energy as well as one of the three transverse gluon modes present in Eq. (1). At intermediate to low temperatures, however, it is actually not known whether this cancellation occurs within the Gribov framework. Unlike the conventional Gribov formalism, this work accounts for medium effects through the Gribov parameter, keeping the number of gluon modes unchanged. This is done on the same footing as HTL perturbation theory, where the medium effect is incorporated via the Debye mass  $m_D$  [77, 78]. Hence, we are considering only two transverse polarizations, and we are deviating from the standard Gribov framework.

Now, the equilibrium pressure and energy density can be obtained from Eq. (2) using the relation

$$\mathcal{P}_{\text{eq}} = -\frac{1}{3} \Delta_{\mu\nu} T_{(0)}^{\mu\nu} = \mathcal{P}_{\text{GZ}} - B_0(T). \quad (5)$$

$$\mathcal{E}_{\text{eq}} = u_\mu u_\nu T_{(0)}^{\mu\nu} = \mathcal{E}_{\text{GZ}} + B_0(T). \quad (6)$$

where  $\Delta_{\mu\nu} = g_{\mu\nu} - u_\mu u_\nu$ ,  $u_\mu$  is the fluid four velocities satisfying  $u^\mu u_\mu = 1$ . In fluid rest frame,  $u^\mu = (1, 0, 0, 0) = (1, \vec{0})$ .  $\mathcal{P}_{\text{GZ}}$  and  $\mathcal{E}_{\text{GZ}}$  are the particle contributions to pressure and energy density of equilibrium Gribov plasma, which gives

$$\mathcal{P}_{\text{GZ}} = \frac{d_g}{(2\pi)^3} \int d^3\mathbf{k} \frac{|\mathbf{k}|^2}{6} \left( \frac{g_+^0}{\epsilon_+} + \frac{g_-^0}{\epsilon_-} \right), \quad (7)$$

$$\mathcal{E}_{\text{GZ}} = \frac{d_g}{(2\pi)^3} \int d^3\mathbf{k} \frac{1}{2} (g_+^0 \epsilon_+ + g_-^0 \epsilon_-). \quad (8)$$

The entropy density of Gribov plasma can be calculated using Eqs. (5) and (6) by utilizing the thermodynamic relation

$$s_{\text{GZ}} = \frac{\mathcal{P}_{\text{GZ}} + \mathcal{E}_{\text{GZ}}}{T} = \frac{\mathcal{P}_{\text{eq}} + \mathcal{E}_{\text{eq}}}{T} = s_{\text{eq}}. \quad (9)$$

where  $s_{\text{eq}}$  denotes the entropy density (for a pure gauge theory) obtained within the Gribov framework. To fix the Gribov parameter, the first step is to match the temperature dependence of the scaled trace anomaly of pure gauge lattice results [79], in order to fix the equilibrium thermodynamic quantities. For analytical tractability, the trace anomaly is fitted with a specific functional form [80]

$$\frac{\mathcal{I}_{\text{eq}}}{T^4} = \frac{\mathcal{I}_{\text{lat}}^F}{T^4} = \exp \left[ - \left( \frac{a_1}{\tilde{T}} + \frac{a_2}{\tilde{T}^2} \right) \right]$$

$$\times \left( \frac{a_0}{1 + a_3 \tilde{T}^2} + \frac{b_0 (\tanh[b_1 \tilde{T} + b_2] + 1)}{1 + c_1 \tilde{T} + c_2 \tilde{T}^2} \right), \quad (10)$$

where  $\tilde{T}$  is the scaled temperature ( $= T/T_c$ ).

$a_0$	$a_1$	$a_2$	$a_3$	$b_0$	$b_1$	$b_2$	$c_1$	$c_2$
0.23	-1.83	2.92	0.07	0.32	62.39	-62.55	-1.98	1.08

**Table 1:** The parameters extracted from the function (Eq. (10)) after fitting with the pure gauge lattice data.

For this set of parameters, the scaled pressure can be obtained by

$$\frac{\mathcal{P}_{\text{eq}}(T)}{T^4} = \frac{\mathcal{P}_{\text{lat}}(T)}{T^4} = \frac{\mathcal{P}_{\text{lat}}(T_{\text{eq}})}{T_{\text{eq}}^4} + \int_{T_{\text{eq}}}^T \frac{d\tilde{T}}{\tilde{T}} \times \frac{\mathcal{I}_{\text{lat}}^F}{\tilde{T}^4}, \quad (11)$$

where  $\mathcal{P}_{\text{lat}}/T_{\text{eq}}^4 = 0.0015$  and  $T_{\text{eq}} = 0.7T_c$ . Following the Eqs. (10) and (11),  $\mathcal{I}_{\text{lat}} = \mathcal{E}_{\text{lat}} - 3\mathcal{P}_{\text{lat}}$  provides the variation of energy density,  $\mathcal{E}_{\text{lat}}$  as a function of scaled temperature. To compute the lattice entropy density  $s_{\text{lat}}$ , we use the thermodynamic relation,  $s_{\text{lat}} = d\mathcal{P}_{\text{lat}}/dT = (\mathcal{P}_{\text{lat}} + \mathcal{E}_{\text{lat}})/T$ . Therefore, using Eq. (9) for the entropy density of the Gribov-modified gluon, we can equate  $s_{\text{GZ}} = s_{\text{lat}}$ , which yields the fixed values of the Gribov parameter as follows in Ref. [74].

Note that for the determination of the Gribov parameter, the thermodynamic matching is performed using pure gauge lattice results, while for the electrical conductivity calculation, we incorporate the quark degrees of freedom in the quasiparticle description, effectively extending the framework towards phenomenological full QCD observables. Thus, the total entropy density of the QGP medium is the sum of the entropy densities of the Gribov-modified gluons and the quasiparticle quarks, i.e

$$s_{\text{total}}^{\text{QGP}} = s_{\text{GZ}}(g) + s_{\text{qp}}(q), \quad (12)$$

where ‘qp(q)’ represents the quasi-particle quark and entropy for qp(q) can be obtained as

$$s_{\text{qp}}(q) = \sum_{i=q,\bar{q}} \frac{d_i}{2\pi^2} \int_0^\infty \mathbf{k}^2 d\mathbf{k} \frac{(\frac{4}{3}\mathbf{k}^2 + m_i^2)}{E_i T} f_i^0. \quad (13)$$

In Eq. (13), the index  $i$  runs over quarks and antiquarks, i.e.,  $i = q, \bar{q}$ . Here the light quark sector consists of  $u$  and  $d$  flavors, while  $s$  denotes the strange quark. The degeneracy factor  $d_i$  accounts for spin and color degrees of freedom and is given by  $d_{q,\bar{q}} = 2 \times N_c \times N_{qt}$  for light quarks (anti-quarks) and  $d_{s,\bar{s}} = 2 \times N_c$  for strange

quarks (anti-quarks), where  $N_c = 3$  and  $N_{ql} = 2$  correspond to the number of colors and light quark flavors, respectively.

$$f_i^0 \equiv f_i^0(E_i, T) = \frac{1}{e^{E_i/T} + 1}, \quad (14)$$

where  $E_i = \sqrt{|\mathbf{k}|^2 + m_i^2}$  is the quasi-particles energies in thermal equilibrium with  $m_i$  as the effective mass. The effective mass depends on the temperature and chemical potential, which arises due to the interaction of quarks and gluons with the surrounding matter and is given by [81]

$$m_i^2 = m_{i0}^2 + \Pi_i, \quad (15)$$

where  $m_{i0}$  is the bare mass and  $\Pi_i$  is the dynamically generated self-energy, which can be obtained by using the hard-thermal loop approximation (HTL) in asymptotic forms as

$$\begin{aligned} \Pi_{ql}(T) &= \frac{g^2 T^2}{3} \left( m_{ql0} \frac{\sqrt{6}}{gT} + 1 \right), \\ \Pi_s(T) &= \frac{g^2 T^2}{3} \left( m_{s0} \frac{\sqrt{6}}{gT} + 1 \right). \end{aligned} \quad (16)$$

where  $m_{ql0}$  and  $m_{s0}$  are the bare masses of the light ( $u, d$ ) and strange ( $s$ ) quarks, whose values are taken as 5 MeV and 95 MeV respectively. Here, we limit our study to the medium at finite temperature and vanishing chemical potential. We are considering the medium, which consists of  $u, d$ , and  $s$  quarks, which interact via the exchange of Gribov-modified gluons.

The interactions of quarks and gluons with the surrounding matter in the medium are encoded in the quasiparticle masses (Eq. 15), which depend on the running coupling,  $g$ . Here, we fix the running coupling using the lattice data of entropy density for (2+1) QCD. The fit function for the entropy density for the medium consisting of the quasiparticle quarks has been formulated much like for the gluonic ( $N_f = 0$ ) case. Therefore, to fix the running coupling, we equated the total entropy density of the QGP medium with the entropy density from the lattice, see Eq. (12).

In Fig. [1], we plot the running coupling,  $g(T)$ , and the scaled Gribov parameter as a function of scaled temperature ( $T/T_c$ ). The critical temperature,  $T_c$ , is taken to be 0.155 GeV. The green line represents the running coupling, and the purple line represents the scaled Gribov parameter. We find that both the Gribov parameter and running coupling decrease monotonically with an increase in temperature above  $T_c$ .

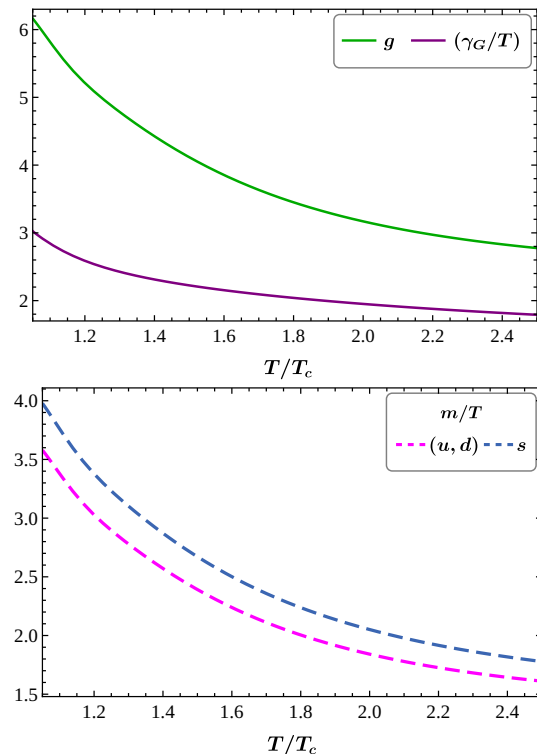


**Fig. 1:** The running coupling  $g(T)$  as a function of  $T/T_c$ , fitted using the lattice equation of state of (2+1)-flavor QCD from Ref. [82]. Also shown are the scaled Gribov parameter  $\gamma_G/T$ , obtained from pure gauge lattice thermodynamics, and the quark quasiparticle masses (Eq. (16)), scaled by temperature, plotted as functions of  $T/T_c$  in the interval  $1.05 \leq T/T_c \leq 2.5$ .

### 3 Elastic cross-sections

To analyze the transport properties of the QGP medium, it is essential to examine the scattering cross-section of its constituent particles. The differential cross-section for the elastic scattering of the type (1+2  $\rightarrow$  3+4) is given as

$$\frac{d\sigma}{dt} = \frac{1}{64\pi s} \frac{1}{p_{\text{cm}}^2} \langle |\mathcal{M}| \rangle_{12 \rightarrow 34}^2, \quad (17)$$

where  $p_{\text{cm}}$  is the momentum in the center of mass (COM) frame of incoming (1,2) and outgoing particles (3,4), which can be calculated as

$$p_{\text{cm}} = \frac{\sqrt{(s - (m_{1,3} - m_{2,4})^2)(s - (m_{1,3} + m_{2,4})^2)}}{2\sqrt{s}}, \quad (18)$$

with  $s$  being the Mandelstam variable. Note that in Eq.(17), the invariant matrix amplitude  $\langle |\mathcal{M}| \rangle_{12 \rightarrow 34}^2$  is averaged over the initial and summed over the final spin states, and are computed perturbatively at the tree level for the elementary two body scattering process among the massive quasiparticle quarks/antiquarks and Gribov modified gluons for various possible channels

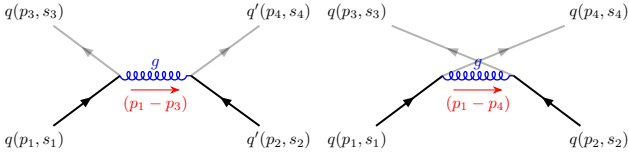


**Fig. 2:** Feynman diagram for  $qq' \rightarrow qq'$  processes. Left:  $t$ -channel and Right:  $u$ -channel, when  $q' = q$ . The black line corresponds to the incoming quarks, while the light grey corresponds to the outgoing quarks. The  $(p_i, s_i)$  is the four-momentum and the spin of the considered quark.

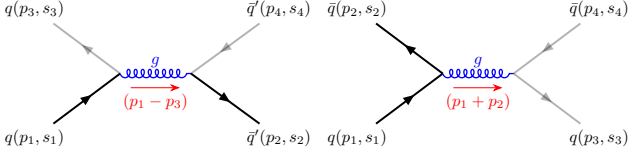


**Fig. 3:** Feynman diagram of  $q\bar{q}' \rightarrow q\bar{q}'$ . Left:  $t$ -channel and Right:  $s$ -channel, when  $\bar{q}' = \bar{q}$ . The black line corresponds to the incoming quark/antiquark, while the light grey corresponds to the outgoing quark/antiquark. The  $(p_i, s_i)$  is the four-momentum and the spin of the considered (anti)quark.

$(s, t, u)$ , as shown in Fig. [2] and Fig. [3]. It is worth noting that even though the higher-order corrections were not considered in the evaluation of the scattering amplitude, those contributions are nevertheless not necessarily small.

The utilization of different symmetries greatly simplifies the task when assessing the invariant scattering amplitudes involving quark-quark and quark-antiquark interactions. Below are a few examples:

- $\langle |\mathcal{M}|^2 \rangle_{d\bar{d} \rightarrow d\bar{d}} = \langle |\mathcal{M}|^2 \rangle_{u\bar{u} \rightarrow u\bar{u}}$ ; (charge symmetry).
- $\langle |\mathcal{M}|^2 \rangle_{d\bar{u} \rightarrow d\bar{u}} = \langle |\mathcal{M}|^2 \rangle_{u\bar{d} \rightarrow u\bar{d}}$ ; (charge conjugation).
- $\langle |\mathcal{M}|^2 \rangle_{u\bar{u} \rightarrow d\bar{d}}(s, t) = \langle |\mathcal{M}|^2 \rangle_{u\bar{d} \rightarrow u\bar{d}}(t, s)$ ; (crossing symmetry).
- $\langle |\mathcal{M}|^2 \rangle_{uu \rightarrow uu}(u, t) = \langle |\mathcal{M}|^2 \rangle_{u\bar{u} \rightarrow u\bar{u}}(s, t)$ ; (crossing symmetry).

The detailed formulation will be presented elsewhere. However, we note that in the limit  $m_{i=1,2,3,4} \rightarrow 0$ , our findings of scattering amplitudes are in line with the one presented in the Ref. [83].

For the process of  $qq(\bar{q}) \rightarrow qq(\bar{q})$ , the total scattering cross-section ( $\sigma_{sc}$ ) can be expressed as

$$\sigma_{sc} = \int_{t_-}^{t_+} dt \left( \frac{d\sigma}{dt} \right) [1 - f_3^0(T)][1 - f_4^0(T)], \quad (19)$$

For  $ug \rightarrow ug$  process, the total scattering cross-section can be written as

$$\sigma_{sc} = \int_{t_-}^{t_+} dt \left( \frac{d\sigma}{dt} \right) [1 - f_3^0(T)][1 + g_4^0(T)], \quad (20)$$

Here,  $(1 - f_{3,4}^0(T))$  and  $(1 + g_4^0(T))$  represent the Pauli blocking/Bose enhancement factors for fermions and

bosons, respectively, these factors take into account the possibility that some of the final states are already occupied with the constituent particles. The functions  $g_i^0$  and  $f_i^0$  represent the equilibrium distribution functions of the “ $i$ th” particles of bosons and fermions, respectively, as defined in Eqs. (3) and (14). The integration limit is fixed by considering the collision in the centre of mass frame, where the Mandelstam variable  $t = -2p_{\text{cm}}^2(1 - \cos\theta)$  with  $-1 \leq \cos\theta \leq 1$ .

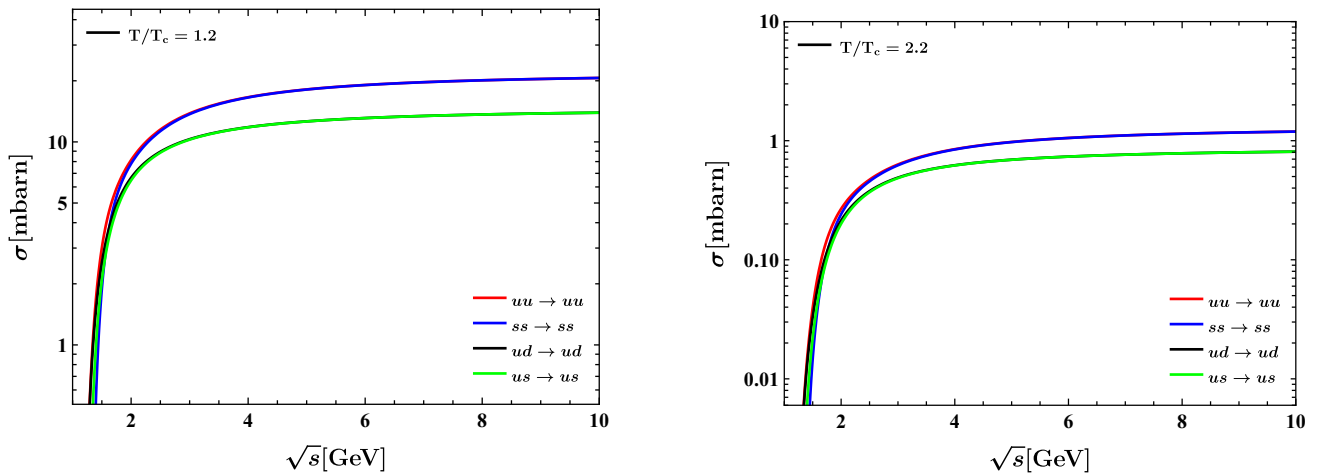
Here, all the partonic cross-sections are fixed as a function of temperature ( $T$ ) and Mandelstam variables ( $s, t, u$ ).

### 3.1 Findings of elastic cross-sections

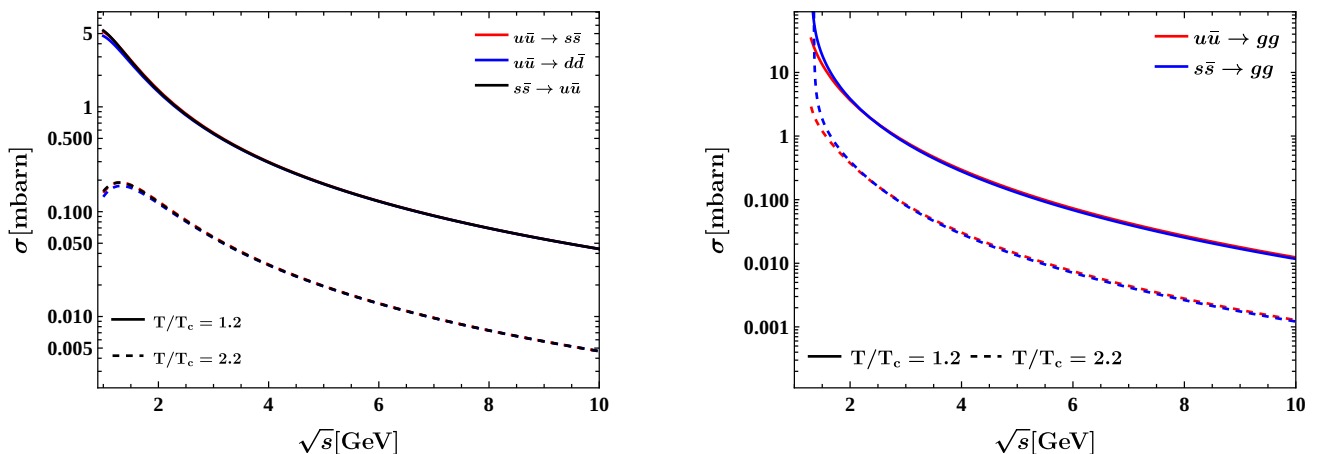
This subsection details the findings regarding the elastic cross-sections for quark-quark, quark-antiquark, and quark-gluon scattering. To provide a comprehensive comparison, we have illustrated each process using plots at two different temperature scales: at  $T/T_c = 1.2$  and  $T/T_c = 2.2$ . It is important to note that we calculated the scattering cross-sections for these processes by using the quasiparticle masses of the quarks, as defined in Eq. (16). Moreover, the interaction among the quarks in the QGP medium occurs via gluon exchange, following the Gribov prescription. We used the modified gluon propagator defined in Eq. (1) to account for this interaction.

The relevant  $2 \rightarrow 2$  scattering processes contributing to the quark relaxation time include quark-quark, quark-antiquark, and quark-gluon scatterings. For the  $u$  quark, these are  $uu \rightarrow uu$  ( $t$ -,  $u$ -channel),  $ud \rightarrow ud$  ( $t$ -channel),  $us \rightarrow us$  ( $t$ -channel),  $u\bar{u} \rightarrow u\bar{u}$  ( $s$ -,  $t$ -channel),  $u\bar{u} \rightarrow d\bar{d}$  ( $s$ -channel),  $u\bar{u} \rightarrow s\bar{s}$  ( $s$ -channel),  $u\bar{d} \rightarrow u\bar{d}$  ( $t$ -channel),  $u\bar{s} \rightarrow u\bar{s}$  ( $t$ -channel),  $ug \rightarrow ug$  ( $t$ -channel), and  $u\bar{u} \rightarrow gg$  ( $s$ -,  $t$ -,  $u$ -channel). The corresponding processes for  $d$  and  $s$  quarks are analogous.

Fig. [4] shows the cross-section for quark-quark scattering as a function of  $\sqrt{s}$  at two different temperatures,  $T/T_c = 1.2$  (left) and  $T/T_c = 2.2$  (right). For a fixed temperature, the scattering cross-section increases with the center-of-mass energy  $\sqrt{s}$ , with a more rapid variation at lower  $\sqrt{s}$ . Specifically, the scattering cross-section increases sharply at smaller values of  $\sqrt{s}$  and then tends to saturate, showing only a weak variation for  $\sqrt{s} \gtrsim 2.5$  GeV. A comparison of the two panels further shows that the overall magnitude of the cross-section decreases as the temperature increases. Interestingly, we observe that the cross-sections are independent of the quasi-masses of the light and strange quarks, and remain the same for both  $q + q \rightarrow q + q$  and  $q + q' \rightarrow q + q'$  processes.



**Fig. 4:** The cross-sections ( $\sigma_{sc}$ ) for the quark-quark scattering are plotted as a function of  $\sqrt{s}$ , with the left plot corresponding to a scaled temperature of  $T/T_c = 1.2$  and the right plot corresponding to  $T/T_c = 2.2$ .



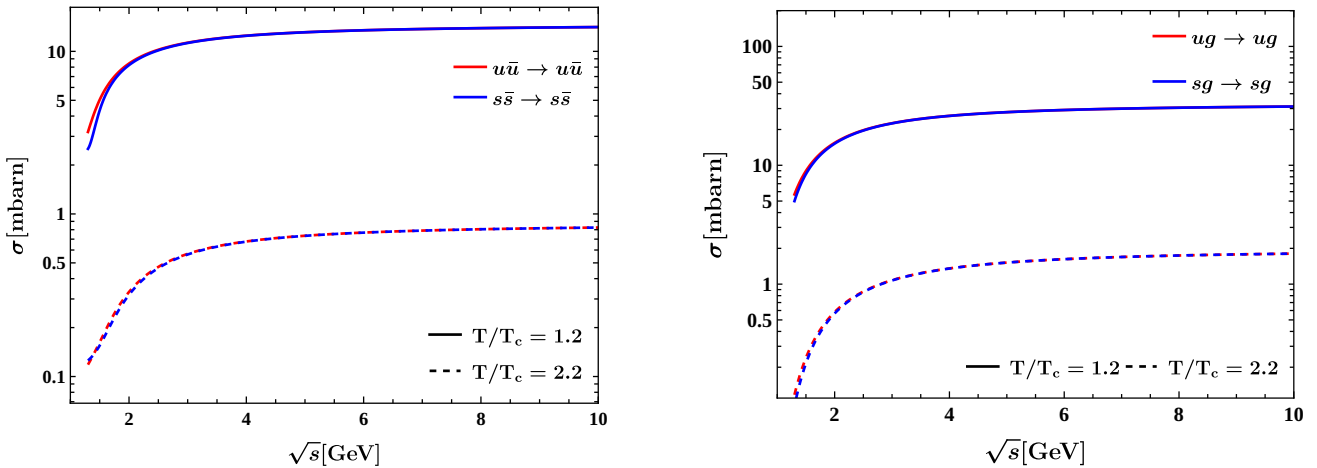
**Fig. 5:** The scattering cross-sections for quark-antiquark (flavor changing) and quark-antiquark pair annihilation as a function of  $\sqrt{s}$  at two different scaled temperatures,  $T/T_c = 1.2$  (solid line) and  $T/T_c = 2.2$  (dashed line)

Fig. [5] demonstrates how the cross-sections vary with the center-of-mass energy ( $\sqrt{s}$ ) for two different processes: flavor-changing quark-antiquark scattering ( $q + \bar{q} \rightarrow q' + \bar{q}'$ ) on the left, and the pair-annihilation of a quark-antiquark pair ( $q + \bar{q} \rightarrow g + g$ ) on the right. As shown in the figure, the scattering cross-section for both processes decreases monotonically as  $\sqrt{s}$  increases. This behavior is in line with the predictions made by the dynamical quasiparticle model [84]. Interestingly, the difference in quasiparticle mass between light and strange quarks has no significant effect on the scattering cross-sections and remains the same for quark-antiquark scattering. Additionally, the difference in quasiparticle mass between light and strange quarks has minimal impact on the cross-sections of their respective pair-annihilations at smaller values of  $\sqrt{s}$ . This observation underscores

the consistent behavior in the scattering process, regardless of the quark flavors involved.

Figure [6] illustrates the behavior of the cross-section for quark-antiquark scattering ( $q + \bar{q} \rightarrow q + \bar{q}$ ) (left) and quark-gluon scattering ( $q + g \rightarrow q + g$ ) (right) as a function of  $\sqrt{s}$ . Notably, for  $\sqrt{s} \geq 3$  GeV, the scattering cross-section remains almost constant for both scaled temperature values,  $T/T_c = 1.2$  (solid line) and  $T/T_c = 2.2$  (dashed line). As the temperature increases, the cross-section value decreases across the entire range of  $\sqrt{s}$ . This trend demonstrates a significant reduction in the scattering cross-section with increasing temperature. It reflects the impact of temperature variations on the dynamics of quark-antiquark pair interaction.

The next step is to formulate the relaxation time ( $\tau_R$ ), which is an essential parameter for calculating the



**Fig. 6:** The cross-sections for the quark-antiquark (no flavor change) (left) and quark-gluon (right) scattering as a function  $\sqrt{s}$ . The solid line corresponds to  $T/T_c = 1.2$  and the dashed line corresponds to  $T/T_c = 2.2$

transport coefficients of the QGP medium, which have been derived using the relaxation time approximation.

#### 4 Relaxation time ( $\tau_R$ )

The transport properties of QGP are largely influenced by the relaxation time,  $\tau_R$ , which plays a crucial role in determining various transport coefficients. Therefore, accurately determining this parameter is of paramount importance in understanding the transport properties of QGP. In this study, we have used the method developed in [85] to calculate the relaxation time,  $\tau_R$ , based on the weighted thermally averaged quark-quark and quark-antiquark cross-sections. A similar approach has been previously used in literature to evaluate the relaxation time  $\tau_R$  [43, 81, 85–87]. The relaxation time for the species “ $i$ ” is given by

$$\tau_i^{-1}(T) = \sum_{j=q,\bar{q},g} n_j(T) \bar{\sigma}_{ij}(s, T), \quad (21)$$

where  $\bar{\sigma}_{ij}$  is the weighted thermal average of the cross-section. In the context of the scattering of the type  $q\bar{q} \rightarrow q'\bar{q}'$ , it is more convenient to define a general notation of the thermally averaged scattering cross-section, which is given as

$$\bar{\sigma}_{12 \rightarrow 34} = \int_{\text{Th}}^{\infty} ds \sigma_{12 \rightarrow 34}(T, s) \mathcal{X}(T, s). \quad (22)$$

Here, the threshold  $\text{Th} = \max\{(m_1 + m_2)^2, (m_3 + m_4)^2\}$  and  $\mathcal{X}(T, s)$  is the probability of finding the quark-quark and quark-antiquark pair with center-of-mass energy  $\sqrt{s}$  [88]

$$\mathcal{X}(T, s) = C \frac{E_1^{\text{cm}}(\sqrt{s} - E_1^{\text{cm}})}{\sqrt{s}} p_{\text{cm}} f_i^0(\sqrt{s} - E_1^{\text{cm}}) f_i^0(E_1^{\text{cm}}), \quad (23)$$

here  $f_i^0(E_i)$  is the fermionic distribution function for quark-(anti) quark scattering as defined in Eq. (14) and  $E_1^{\text{cm}}$  is defined as

$$E_1^{\text{cm}}(s, T) = \frac{s - (m_1(T)^2 - m_2(T)^2)}{2\sqrt{s}}. \quad (24)$$

Note that the normalization in Eq. (23) is fixed by

$$[\mathcal{C}(T)]^{-1} = \int_{\text{Th}}^{\infty} ds \mathcal{X}(T, s). \quad (25)$$

Note that the electrical conductivity is primarily governed by the transport of electrically charged quarks. Since gluons are electrically neutral, they do not couple directly to the external electromagnetic field and therefore do not contribute independently to the electrical current. Their role enters indirectly through quark-gluon scattering processes, which affect the relaxation time of quarks. The relaxation time for the light quarks is obtained as [86]

$$\begin{aligned} \tau_u^{-1}(T) = & n_{\bar{u}}(\bar{\sigma}_{u\bar{u} \rightarrow u\bar{u}} + \bar{\sigma}_{u\bar{u} \rightarrow d\bar{d}} + \bar{\sigma}_{u\bar{u} \rightarrow s\bar{s}} + \bar{\sigma}_{u\bar{d} \rightarrow u\bar{d}} \\ & + \bar{\sigma}_{u\bar{u} \rightarrow g g}) + n_u(\bar{\sigma}_{uu \rightarrow uu} + \bar{\sigma}_{ud \rightarrow ud}) + n_s \bar{\sigma}_{us \rightarrow us} \\ & + n_{\bar{s}} \bar{\sigma}_{u\bar{s} \rightarrow u\bar{s}} + n_g \bar{\sigma}_{ug \rightarrow ug}, \end{aligned} \quad (26)$$

and for the strange quark is

$$\begin{aligned} \tau_s^{-1}(T) = & 2n_u \bar{\sigma}_{us \rightarrow us} + 2n_{\bar{u}} \bar{\sigma}_{u\bar{s} \rightarrow u\bar{s}} + n_s \bar{\sigma}_{ss \rightarrow ss} + \\ & n_{\bar{s}}(\bar{\sigma}_{s\bar{s} \rightarrow s\bar{s}} + \bar{\sigma}_{s\bar{s} \rightarrow g g} + 2\bar{\sigma}_{s\bar{s} \rightarrow u\bar{u}}) + n_g \bar{\sigma}_{sg \rightarrow sg}, \end{aligned} \quad (27)$$

Here  $\bar{\sigma}_{12 \rightarrow 34}$  is the weighted thermally averaged cross sections, as defined in Eq. (22). In Eq. (26) and Eq. (27),  $n_i(T)$  is the equilibrium number density of the particles, which is defined for quarks as

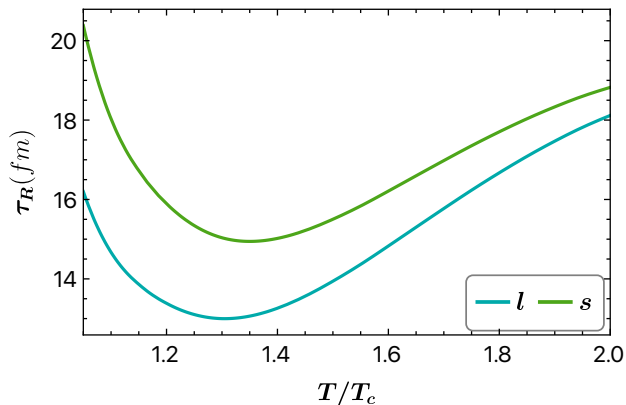


**Fig. 7:** The relaxation time ( $\tau_R$ ) as a function of the scaled temperature for the light (Eq. 26) and strange quarks (Eq. 27). The light quark consists of  $u$  and  $d$  quarks.

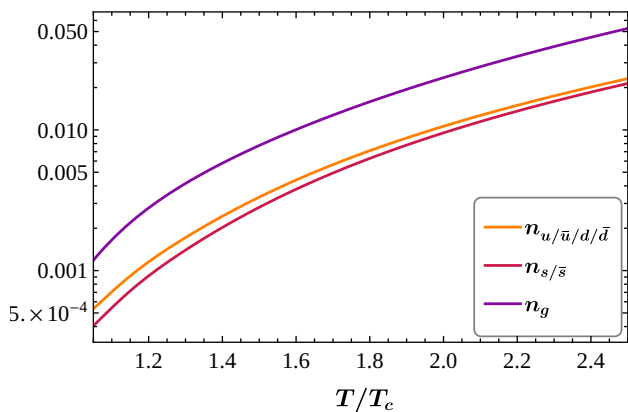


**Fig. 8:** The equilibrium number density of the light and strange quark along with Gribov modified gluons as a function of  $T/T_c$  in the range  $1.05 \leq T/T_c \leq 2.5$ .

$$n_i(T) = d_i \int \frac{d^3 p_i}{(2\pi)^3} f_i^0, \quad (28)$$

and for gluons as

$$n_g(T) = d_g \int \frac{d^3 p}{(2\pi)^3} g^0. \quad (29)$$

Here,  $f_i^0$  is the equilibrium distribution function for quarks as defined in Eq. (14), while  $g^0$  is the equilibrium distribution function for the Gribov modified gluons, with  $g_{\pm}^0$  corresponding to the two dispersion branches as mentioned in Eq. (3). In Fig. [7], we present the behavior of relaxation times as a function of scaled temperature. It is measured at vanishing chemical potential. It is observed that the relaxation time for both light and strange quarks first decreases and then increases with temperature. In Fig. [8], the variation of the number densities of the light quarks and the strange quark is plotted against the scaled temperature  $T/T_c$ . We see that the number density of the Gribov modified gluons

is significantly higher compared to quasiparticle quarks for the entire range of scaled temperature.

## 5 Electrical conductivity

In this section, we have computed the electrical conductivity of the QGP medium, which quantifies the ability of a system to conduct electric charges. After solving the relativistic Boltzmann kinetic equation in the relaxation time approximation (RTA), one can obtain the electrical conductivity expression as [42, 89]

$$\sigma_{\text{el}} = \frac{1}{3T} \sum_{i=q,\bar{q}} \int \frac{d^3 k}{(2\pi)^3} \frac{k^2}{E_i^2} q_i^2 d_i \tau_i f_i^0 (1 - f_i^0), \quad (30)$$

where  $\tau_i$  is the relaxation time of the  $i$ -th quark or antiquark species, defined in Section 4. The electric charge  $q_i$  for  $u$ ,  $d$  and  $s$  quarks are  $q_u = -q_{\bar{u}} = 2e/3$  and  $q_{d,s} = -q_{\bar{d},\bar{s}} = -e/3$ , respectively. The electron charge  $e = \sqrt{4\pi\alpha}$  with the fine structure constant,  $\alpha = 1/137$  and  $f_i^0$  is the equilibrium distribution, which is defined in Eq. (14). In Fig. [9], we present a plot of the electrical conductivity as a function of scaled temperature. The plot on top compares our electrical conductivity results for different flavors ( $l$ ,  $s$ , and  $N_f = (2 + 1)$ ) with the lattice data [31]. The red, blue, and green dashed lines correspond to the light (consisting of  $u$  and  $d$  quarks), strange, and  $N_f = (2 + 1)$  flavors, respectively, along with the same color symbols taken from the lattice data.

In plot on the bottom, we show the variation of the electrical conductivity for  $N_f = (2 + 1)$  (solid red line) compared with the results from the Quasiparticle Model (QPM) (blue and yellow dashed lines) [36, 89], lattice QCD (red circle), and the black dot-dashed line represents the value of  $\sigma/T = e^2 N_c^2 / 16\pi \sim 0.017$  obtained using the AdS/CFT approach [90]. Our results are in close agreement with the lattice data. It is worth mentioning that the antiquark contribution to the electrical conductivity ( $\sigma_{u,d,s}$ ) has been neglected while comparing our findings with those of the lattice calculation of the same, considering that the lattice findings do not include the contribution from respective antiquarks, and are just for quarks.

## 6 Summary and outlook

In this work, we have investigated the electrical conductivity scaled with temperature  $T$  for the medium QGP, consisting of light ( $u$  and  $d$ ) and strange quarks, using the quasiparticle approach within the kinetic theory framework in relaxation time approximation. The exchanged gluons between quarks are modified by the Gribov prescription, where the temperature dependence of

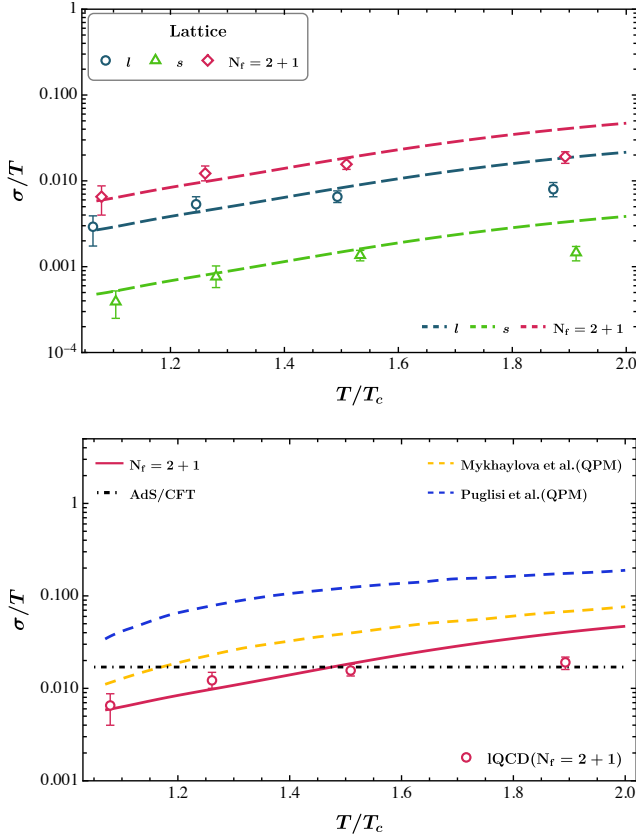


**Fig. 9:** The scaled electrical conductivity as a function of the scaled temperature for different flavors ( $l$ ,  $s$ , and  $N_f = (2 + 1)$ ) (left) and for  $N_f = (2 + 1)$  (right). The blue, green, and red symbols from lattice data [31], blue and yellow lines from QPM [36, 89], and the black dot-dashed line from the AdS/CFT approach [90].

the Gribov parameter is fixed from pure gauge lattice thermodynamics. Also, the quasi-masses of the light and strange quarks are parameterised with the running coupling  $g(T)$ , which is obtained using the lattice equation of state of  $(2 + 1)$ -flavor QCD.

The relaxation time  $\tau_R$  has been an important dynamical parameter in determining the transport coefficients, including the electrical conductivity. In this work, the relaxation time has been evaluated using the thermally averaged cross-section of all possible quark-(anti)quark scatterings to the lowest order; however, it is worth noting that higher-order corrections may have a significant impact on the outcome.

We also investigated the quark flavor dependence of the electrical conductivity and compared it with the available lattice findings. We observe a good match with the lattice data, particularly near the phase transition temperature. We also compared our final result with the previous finding of the electrical conductivity based on the quasiparticle model.

## Acknowledgements

Discussion with Aritra Bandhopadhyay and Hiranmay Mishra is highly appreciated. L. T. is supported by the National Research Foundation (NRF) funded by the Ministry of Science of Korea (Grant No. 2021R1F1A1061387). N.H. is supported in part by the SERB-MATRICES under Grant No. MTR/2021/000939

## References

1. M. Gyulassy and L. McLerran, “New forms of QCD matter discovered at RHIC,” Nucl. Phys. A **750**, 30-63 (2005) <https://doi.org/10.1016/j.nuclphysa.2004.10.034>
2. P. Jacobs and X. N. Wang, “Matter in extremis: Ultrarelativistic nuclear collisions at RHIC,” Prog. Part. Nucl. Phys. **54**, 443-534 (2005) <https://doi.org/10.1016/j.ppnp.2004.09.001>
3. W. Busza, K. Rajagopal and W. van der Schee, “Heavy Ion Collisions: The Big Picture, and the Big Questions,” Ann. Rev. Nucl. Part. Sci. **68**, 339-376 (2018) <https://doi.org/10.1146/annurev-nucl-101917-020852>
4. D. Teaney, J. Lauret and E. V. Shuryak, “Flow at the SPS and RHIC as a quark gluon plasma signature,” Phys. Rev. Lett. **86**, 4783-4786 (2001) <https://doi.org/10.1103/PhysRevLett.86.4783>
5. P. Huovinen, P. F. Kolb, U. W. Heinz, P. V. Ruuskanen and S. A. Voloshin, “Radial and elliptic flow at RHIC: Further predictions,” Phys. Lett. B **503**, 58-64 (2001) [https://doi.org/10.1016/S0370-2693\(01\)00219-2](https://doi.org/10.1016/S0370-2693(01)00219-2)
6. T. Hirano and K. Tsuda, “Collective flow and two pion correlations from a relativistic hydrodynamic model with early chemical freezeout,” Phys. Rev. C **66**, 054905 (2002) <https://doi.org/10.1103/PhysRevC.66.054905>
7. W. Broniowski, M. Chojnacki, W. Florkowski and A. Kisiel, “Uniform Description of Soft Observables in Heavy-Ion Collisions at  $s(\text{NN})^{1/2} = 200 \text{ GeV}^2$ ,” Phys. Rev. Lett. **101**, 022301 (2008) <https://doi.org/10.1103/PhysRevLett.101.022301>
8. B. Schenke, S. Jeon and C. Gale, “(3+1)D hydrodynamic simulation of relativistic heavy-ion collisions,” Phys. Rev. C **82**, 014903 (2010) <https://doi.org/10.1103/PhysRevC.82.014903>
9. P. Romatschke and U. Romatschke, “Viscosity Information from Relativistic Nuclear Collisions: How Perfect is the Fluid Observed at RHIC?,” Phys. Rev. Lett. **99**, 172301 (2007) <https://doi.org/10.1103/PhysRevLett.99.172301>

10. H. Song and U. W. Heinz, "Suppression of elliptic flow in a minimally viscous quark-gluon plasma," *Phys. Lett. B* **658**, 279-283 (2008) <https://doi.org/10.1016/j.physletb.2007.11.019>
11. K. Dusling and D. Teaney, "Simulating elliptic flow with viscous hydrodynamics," *Phys. Rev. C* **77**, 034905 (2008) <https://doi.org/10.1103/PhysRevC.77.034905>
12. P. Bozek, "Bulk and shear viscosities of matter created in relativistic heavy-ion collisions," *Phys. Rev. C* **81**, 034909 (2010) <https://doi.org/10.1103/PhysRevC.81.034909>
13. P. Bozek and I. Wykiel-Piekarska, "Particle spectra in Pb-Pb collisions at  $\sqrt{s_{NN}} = 2.76$  TeV," *Phys. Rev. C* **85**, 064915 (2012) <https://doi.org/10.1103/PhysRevC.85.064915>
14. S. Ryu, J. F. Paquet, C. Shen, G. S. Denicol, B. Schenke, S. Jeon and C. Gale, "Importance of the Bulk Viscosity of QCD in Ultrarelativistic Heavy-Ion Collisions," *Phys. Rev. Lett.* **115**, no.13, 132301 (2015) <https://doi.org/10.1103/PhysRevLett.115.132301>
15. L. Du and U. Heinz, "(3+1)-dimensional dissipative relativistic fluid dynamics at non-zero net baryon density," *Comput. Phys. Commun.* **251**, 107090 (2020) <https://doi.org/10.1016/j.cpc.2019.107090>
16. H. B. Meyer, "A Calculation of the bulk viscosity in SU(3) gluodynamics," *Phys. Rev. Lett.* **100**, 162001 (2008) <https://doi.org/10.1103/PhysRevLett.100.162001>
17. U. Heinz and R. Snellings, "Collective flow and viscosity in relativistic heavy-ion collisions," *Ann. Rev. Nucl. Part. Sci.* **63**, 123-151 (2013) <https://doi.org/10.1146/annurev-nucl-102212-170540>
18. S. Jeon and U. Heinz, "Introduction to Hydrodynamics," *Int. J. Mod. Phys. E* **24**, no.10, 1530010 (2015) <https://doi.org/10.1142/S0218301315300106>
19. C. Gale, S. Jeon and B. Schenke, "Hydrodynamic Modeling of Heavy-Ion Collisions," *Int. J. Mod. Phys. A* **28** (2013), 1340011 <https://doi.org/10.1016/10.1142/S0217751X13400113>
20. B. Schenke, S. Jeon and C. Gale, "Elliptic and triangular flows in 3 + 1D viscous hydrodynamics with fluctuating initial conditions," *J. Phys. G* **38** (2011), 124169 <https://doi.org/10.1088/0954-3899/38/12/124169>
21. K. Tuchin, "Particle production in strong electromagnetic fields in relativistic heavy-ion collisions," *Adv. High Energy Phys.* **2013** (2013), 490495 <https://doi.org/10.1155/2013/490495>
22. P. B. Arnold, G. D. Moore and L. G. Yaffe, "Transport coefficients in high temperature gauge theories. 1. Leading log results," *JHEP* **11** (2000), 001 <https://doi.org/10.1088/1126-6708/2000/11/001>
23. P. B. Arnold, G. D. Moore and L. G. Yaffe, "Transport coefficients in high temperature gauge theories. 2. Beyond leading log," *JHEP* **05** (2003), 051 <https://doi.org/10.1088/1126-6708/2003/05/051>
24. S. Gupta, "The Electrical conductivity and soft photon emissivity of the QCD plasma," *Phys. Lett. B* **597** (2004), 57-62 <https://doi.org/10.1016/j.physletb.2004.05.079>
25. G. Aarts, C. Allton, J. Foley, S. Hands and S. Kim, "Spectral functions at small energies and the electrical conductivity in hot, quenched lattice QCD," *Phys. Rev. Lett.* **99** (2007), 022002 <https://doi.org/10.1103/PhysRevLett.99.022002>
26. P. V. Buividovich, M. N. Chernodub, D. E. Kharzeev, T. Kalaydzhyan, E. V. Luschevskaya and M. I. Polikarpov, "Magnetic-Field-Induced insulator-conductor transition in SU(2) quenched lattice gauge theory," *Phys. Rev. Lett.* **105** (2010), 132001 <https://doi.org/10.1103/PhysRevLett.105.132001>
27. H. T. Ding, A. Francis, O. Kaczmarek, F. Karsch, E. Laermann and W. Soeldner, "Thermal dilepton rate and electrical conductivity: An analysis of vector current correlation functions in quenched lattice QCD," *Phys. Rev. D* **83** (2011), 034504 <https://doi.org/10.1103/PhysRevD.83.034504>
28. Y. Burnier and M. Laine, "Towards flavour diffusion coefficient and electrical conductivity without ultraviolet contamination," *Eur. Phys. J. C* **72** (2012), 1902 <https://doi.org/10.1140/epjc/s10052-012-1902-8>
29. B. B. Brandt, A. Francis, H. B. Meyer and H. Wittig, "Thermal Correlators in the  $\rho$  channel of two-flavor QCD," *JHEP* **03** (2013), 100 [https://doi.org/10.1007/JHEP03\(2013\)100](https://doi.org/10.1007/JHEP03(2013)100)
30. A. Amato, G. Aarts, C. Allton, P. Giudice, S. Hands and J. I. Skullerud, "Electrical conductivity of the quark-gluon plasma across the deconfinement transition," *Phys. Rev. Lett.* **111** (2013) no.17, 172001 <https://doi.org/10.1103/PhysRevLett.111.172001>
31. G. Aarts, C. Allton, A. Amato, P. Giudice, S. Hands and J. I. Skullerud, "Electrical conductivity and charge diffusion in thermal QCD from the lattice," *JHEP* **02** (2015), 186 [https://doi.org/10.1007/JHEP02\(2015\)186](https://doi.org/10.1007/JHEP02(2015)186)
32. W. Cassing, O. Linnyk, T. Steinert and V. Ozvenchuk, "Electrical Conductivity of Hot QCD Matter," *Phys.*

- Rev. Lett. **110** (2013) no.18, 182301  
<https://doi.org/10.1103/PhysRevLett.110.182301>
33. T. Steinert and W. Cassing, “Electric and magnetic response of hot QCD matter,” Phys. Rev. C **89** (2014) no.3, 035203  
<https://doi.org/10.1103/PhysRevC.89.035203>
  34. Y. Hirono, M. Hongo and T. Hirano, “Estimation of electric conductivity of the quark gluon plasma via asymmetric heavy-ion collisions,” Phys. Rev. C **90** (2014) no.2, 021903  
<https://doi.org/10.1103/PhysRevC.90.021903>
  35. M. Greif, I. Bouras, C. Greiner and Z. Xu, “Electric conductivity of the quark-gluon plasma investigated using a perturbative QCD based parton cascade,” Phys. Rev. D **90** (2014) no.9, 094014  
<https://doi.org/10.1103/PhysRevD.90.094014>
  36. A. Puglisi, S. Plumari and V. Greco, “Shear viscosity  $\eta$  to electric conductivity  $\sigma_{el}$  ratio for the quark-gluon plasma,” Phys. Lett. B **751** (2015), 326-330  
<https://doi.org/10.1016/j.physletb.2015.10.070>
  37. A. Puglisi, S. Plumari and V. Greco, “Electric Conductivity from the solution of the Relativistic Boltzmann Equation,” Phys. Rev. D **90** (2014), 114009  
<https://doi.org/10.1103/PhysRevD.90.114009>
  38. S. I. Finazzo and J. Noronha, “Holographic calculation of the electric conductivity of the strongly coupled quark-gluon plasma near the deconfinement transition,” Phys. Rev. D **89** (2014) no.10, 106008  
<https://doi.org/10.1103/PhysRevD.89.106008>
  39. M. Greif, C. Greiner and G. S. Denicol, “Electric conductivity of a hot hadron gas from a kinetic approach,” Phys. Rev. D **93** (2016) no.9, 096012 [erratum: Phys. Rev. D **96** (2017) no.5, 059902]  
<https://doi.org/10.1103/PhysRevD.93.096012>
  40. S. Mitra and V. Chandra, “Thermal relaxation, electrical conductivity, and charge diffusion in a hot QCD medium,” Phys. Rev. D **94** (2016) no.3, 034025  
<https://doi.org/10.1103/PhysRevD.94.034025>
  41. P. K. Srivastava, L. Thakur and B. K. Patra, “Electrical Conductivity of an Anisotropic Quark Gluon Plasma : A Quasiparticle Approach,” Phys. Rev. C **91** (2015) no.4, 044903  
<https://doi.org/10.1103/PhysRevC.91.044903>
  42. L. Thakur, P. K. Srivastava, G. P. Kadam, M. George and H. Mishra, “Shear viscosity  $\eta$  to electrical conductivity  $\sigma_{el}$  ratio for an anisotropic QGP,” Phys. Rev. D **95** (2017) no.9, 096009  
<https://doi.org/10.1103/PhysRevD.95.096009>
  43. R. Marty, E. Bratkovskaya, W. Cassing, J. Aichelin and H. Berrehrh, “Transport coefficients from the Nambu-Jona-Lasinio model for  $SU(3)_f$ ,” Phys. Rev. C **88** (2013), 045204  
<https://doi.org/10.1103/PhysRevC.88.045204>
  44. G. P. Kadam, H. Mishra and L. Thakur, “Electrical and thermal conductivities of hot and dense hadronic matter,” Phys. Rev. D **98** (2018) no.11, 114001  
<https://doi.org/10.1103/PhysRevD.98.114001>
  45. L. Thakur and P. K. Srivastava, “Electrical conductivity of a hot and dense QGP medium in a magnetic field,” Phys. Rev. D **100**, no.7, 076016 (2019)  
<https://doi.org/10.1103/PhysRevD.100.076016>
  46. H. Berrehrh, E. Bratkovskaya, T. Steinert and W. Cassing, “A dynamical quasiparticle approach for the QGP bulk and transport properties,” Int. J. Mod. Phys. E **25**, no.07, 1642003 (2016)  
<https://doi.org/10.1142/S0218301316420039>
  47. S. Mitra and V. Chandra, “Covariant kinetic theory for effective fugacity quasiparticle model and first order transport coefficients for hot QCD matter,” Phys. Rev. D **97**, no.3, 034032 (2018)  
<https://doi.org/10.1103/PhysRevD.97.034032>
  48. O. Soloveva, P. Moreau and E. Bratkovskaya, “Transport coefficients for the hot quark-gluon plasma at finite chemical potential  $\mu_B$ ,” Phys. Rev. C **101**, no.4, 045203 (2020)  
<https://doi.org/10.1103/PhysRevC.101.045203>
  49. P. Singha, A. Abhishek, G. Kadam, S. Ghosh and H. Mishra, “Calculations of shear, bulk viscosities and electrical conductivity in the Polyakov-quark-meson model,” J. Phys. G **46**, no.1, 015201 (2019) <https://doi.org/10.1088/1361-6471/aaf256>
  50. S. Mitra and V. Chandra, “Transport coefficients of a hot QCD medium and their relative significance in heavy-ion collisions,” Phys. Rev. D **96**, no.9, 094003 (2017)  
<https://doi.org/10.1103/PhysRevD.96.094003>
  51. R. Ghosh and I. A. Shovkovy, “Electrical conductivity of hot relativistic plasma in a strong magnetic field,” Phys. Rev. D **110** (2024) no.9, 9  
<https://doi.org/10.1103/PhysRevD.110.096009>
  52. K. Fukushima, D. E. Kharzeev and H. J. Warringa, “The Chiral Magnetic Effect,” Phys. Rev. D **78** (2008), 074033  
<https://doi.org/10.1103/PhysRevD.78.074033>
  53. D. E. Kharzeev, L. D. McLerran and H. J. Warringa, “The Effects of topological charge change in heavy ion collisions: ‘Event by event P and CP violation’,” Nucl. Phys. A **803** (2008), 227-253  
<https://doi.org/10.1016/j.nuclphysa.2008.02.298>
  54. S. Turbide, R. Rapp and C. Gale, “Hadronic production of thermal photons,” Phys. Rev. C **69**, 014903 (2004)

- <https://doi.org/10.1103/PhysRevC.69.014903>
55. O. Linnyk, W. Cassing and E. L. Bratkovskaya, “Centrality dependence of the direct photon yield and elliptic flow in heavy-ion collisions at  $\sqrt{s_{NN}} = 200$  GeV,” *Phys. Rev. C* **89**, no.3, 034908 (2014) <https://doi.org/10.1103/PhysRevC.89.034908>
  56. V. N. Gribov, “Quantization of Nonabelian Gauge Theories,” *Nucl. Phys. B* **139** (1978), 1 [https://doi.org/10.1016/0550-3213\(78\)90175-X](https://doi.org/10.1016/0550-3213(78)90175-X)
  57. D. Zwanziger, “Local and Renormalizable Action From the Gribov Horizon,” *Nucl. Phys. B* **323**, 513-544 (1989). [https://doi.org/10.1016/0550-3213\(89\)90122-3](https://doi.org/10.1016/0550-3213(89)90122-3)
  58. D. Zwanziger, “Equation of state of gluon plasma from fundamental modular region,” *Phys. Rev. Lett.* **94**, 182301 (2005) <https://doi.org/10.1103/PhysRevLett.94.182301>
  59. D. Zwanziger, “Equation of State of Gluon Plasma from Local Action,” *Phys. Rev. D* **76**, 125014 (2007) <https://doi.org/10.1103/PhysRevD.76.125014>
  60. K. Fukushima and N. Su, “Stabilizing perturbative Yang-Mills thermodynamics with Gribov quantization,” *Phys. Rev. D* **88**, 076008 (2013) <https://doi.org/10.1103/PhysRevD.88.076008>
  61. N. Su and K. Tywoniuk, “Massless Mode and Positivity Violation in Hot QCD,” *Phys. Rev. Lett.* **114**, no.16, 161601 (2015) <https://doi.org/10.1103/PhysRevLett.114.161601>
  62. W. Florkowski, R. Ryblewski, N. Su and K. Tywoniuk, “Transport coefficients of the Gribov-Zwanziger plasma,” *Phys. Rev. C* **94**, no.4, 044904 (2016) <https://doi.org/10.1103/PhysRevC.94.044904>
  63. W. Florkowski, R. Ryblewski, N. Su and K. Tywoniuk, “Bulk viscosity in a plasma of Gribov-Zwanziger gluons,” *Acta Phys. Polon. B* **47**, 1833 (2016) <https://doi.org/10.5506/APhysPolB.47.1833>
  64. V. Begun, W. Florkowski and R. Ryblewski, “Thermodynamics and kinetics of Gribov-Zwanziger plasma with temperature dependent Gribov parameter,” *Acta Phys. Polon. B* **48**, 125 (2017) <https://doi.org/10.5506/APhysPolB.48.125>
  65. A. Bandyopadhyay, N. Haque, M. G. Mustafa and M. Strickland, “Dilepton rate and quark number susceptibility with the Gribov action,” *Phys. Rev. D* **93**, no.6, 065004 (2016) <https://doi.org/10.1103/PhysRevD.93.065004>
  66. S. Madni, A. Mukherjee, A. Jaiswal and N. Haque, “Shear and bulk viscosity of the quark-gluon plasma with Gribov gluons and quasiparticle quarks,” *Phys. Rev. D* **110** (2024) no.11, 116035 <https://doi.org/10.1103/PhysRevD.110.116035>
  67. Sumit, N. Haque and B. K. Patra, “QCD mesonic screening masses using Gribov quantization,” *Phys. Lett. B* **845**, 138143 (2023) <https://doi.org/10.1016/j.physletb.2023.138143>
  68. Y. L. Du, N. Su and K. Tywoniuk, “Spectral sum rules and phase transition in strongly coupled QCD,” [arXiv:2412.20165 [hep-th]]. arXiv:2412.20165 [hep-th]
  69. M. Debnath, R. Ghosh and N. Haque, “The complex heavy quarkonium potential with the Gribov-Zwanziger action,” *Eur. Phys. J. C* **84** (2024) no.3, 313 <https://doi.org/10.1140/epjc/s10052-024-12656-2>
  70. S. Madni, A. Mukherjee, A. Bandyopadhyay and N. Haque, “Estimation of the diffusion coefficient of heavy quarks in light of Gribov-Zwanziger action,” *Phys. Lett. B* **838**, 137714 (2023) <https://doi.org/10.1016/j.physletb.2023.137714>
  71. Sumit, A. Mukherjee, N. Haque and B. K. Patra, “Heavy quark dynamics via the Gribov-Zwanziger approach,” *Phys. Rev. D* **109** (2024) no.11, 114043 <https://doi.org/10.1103/PhysRevD.109.114043>
  72. Sumit, J. Prakash, S. K. Das and N. Haque, “Anisotropy effects on heavy quark dynamics in Gribov modified gluon plasma,” [arXiv:2506.01922 [hep-ph]]. arXiv:2506.01922 [hep-ph]
  73. S. Mazumder, N. Sharma and L. Kumar, “Transport coefficients of the heavy quark in the domain of the nonperturbative and noneikonal gluon radiation,” *Phys. Rev. C* **111** (2025) no.3, 034905 <https://doi.org/10.1103/PhysRevC.111.034905>
  74. A. Jaiswal and N. Haque, “Covariant kinetic theory and transport coefficients for Gribov plasma,” *Phys. Lett. B* **811**, 135936 (2020) <https://doi.org/10.1016/j.physletb.2020.135936>
  75. S. Jeon and L. G. Yaffe, “From quantum field theory to hydrodynamics: Transport coefficients and effective kinetic theory,” *Phys. Rev. D* **53** (1996), 5799-5809 <https://doi.org/10.1103/PhysRevD.53.5799>
  76. D. Dudal, J. A. Gracey, S. P. Sorella, N. Vandersickel and H. Verschelde, “A Refinement of the Gribov-Zwanziger approach in the Landau gauge: Infrared propagators in harmony with the lattice results,” *Phys. Rev. D* **78**, 065047 (2008) <https://doi.org/10.1103/PhysRevD.78.065047>
  77. J. Ghiglieri, A. Kurkela, M. Strickland and A. Vuorinen, “Perturbative Thermal QCD: Formalism and Applications,” *Phys. Rept.* **880** (2020), 1-73 <https://doi.org/10.1016/j.physrep.2020.07.004>
  78. N. Haque and M. G. Mustafa, “Hard Thermal Loop—Theory and applications,”

- Prog. Part. Nucl. Phys. **140** (2025), 104136  
<https://doi.org/10.1016/j.pnpnp.2024.104136>
79. S. Borsanyi, G. Endrodi, Z. Fodor, S. D. Katz and K. K. Szabo, "Precision SU(3) lattice thermodynamics for a large temperature range," JHEP **07**, 056 (2012)  
[https://doi.org/10.1007/JHEP07\(2012\)056](https://doi.org/10.1007/JHEP07(2012)056)
80. S. Borsanyi, G. Endrodi, Z. Fodor, A. Jaksz, S. D. Katz, S. Krieg, C. Ratti and K. K. Szabo, "The QCD equation of state with dynamical quarks," JHEP **11**, 077 (2010)  
[https://doi.org/10.1007/JHEP11\(2010\)077](https://doi.org/10.1007/JHEP11(2010)077)
81. V. Mykhaylova, M. Bluhm, K. Redlich and C. Sasaki, "Quark-flavor dependence of the shear viscosity in a quasiparticle model," Phys. Rev. D **100**, no.3, 034002 (2019)  
<https://doi.org/10.1103/PhysRevD.100.034002>
82. S. Borsanyi, Z. Fodor, C. Hoelbling, S. D. Katz, S. Krieg and K. K. Szabo, "Full result for the QCD equation of state with 2+1 flavors," Phys. Lett. B **730**, 99-104 (2014)  
<https://doi.org/10.1016/j.physletb.2014.01.007>
83. R. Cutler and D. W. Sivers, "Quantum Chromodynamic Gluon Contributions to Large p(T) Reactions," Phys. Rev. D **17**, 196 (1978)  
<https://doi.org/10.1103/PhysRevD.17.196>
84. P. Moreau, O. Soloveva, L. Oliva, T. Song, W. Cassing and E. Bratkovskaya, "Exploring the partonic phase at finite chemical potential within an extended off-shell transport approach," Phys. Rev. C **100**, no.1, 014911 (2019)  
<https://doi.org/10.1103/PhysRevC.100.014911>
85. C. Sasaki and K. Redlich, "Transport coefficients near chiral phase transition," Nucl. Phys. A **832**, 62-75 (2010)  
<https://doi.org/10.1016/j.nuclphysa.2009.11.005>
86. O. Soloveva, D. Fuseau, J. Aichelin and E. Bratkovskaya, "Shear viscosity and electric conductivity of a hot and dense QGP with a chiral phase transition," Phys. Rev. C **103**, no.5, 054901 (2021)  
<https://doi.org/10.1103/PhysRevC.103.054901>
87. P. Danielewicz and M. Gyulassy, "Dissipative Phenomena in Quark Gluon Plasmas," Phys. Rev. D **31**, 53-62 (1985)  
<https://doi.org/10.1103/PhysRevD.31.53>
88. H. Berrehrah, E. Bratkovskaya, W. Cassing, P. B. Gossiaux, J. Aichelin and M. Bleicher, "Collisional processes of on-shell and off-shell heavy quarks in vacuum and in the Quark-Gluon-Plasma," Phys. Rev. C **89**, no.5, 054901 (2014)  
<https://doi.org/10.1103/PhysRevC.89.054901>
89. V. Mykhaylova and C. Sasaki, "Impact of quark quasiparticles on transport coefficients in hot QCD," Phys. Rev. D **103**, no.1, 014007 (2021)  
<https://doi.org/10.1103/PhysRevD.103.014007>
90. S. Caron-Huot, P. Kovtun, G. D. Moore, A. Starinets and L. G. Yaffe, "Photon and dilepton production in supersymmetric Yang-Mills plasma," JHEP **12**, 015 (2006)  
<https://doi.org/10.1088/1126-6708/2006/12/015>